Colloids and Surfaces A: Physicochemical and Engineering Aspects 669 (2023) 131493

Contents lists available at ScienceDirect

Colloids and Surfaces A: Physicochemical and Engineering Aspects

journal homepage: www.elsevier.com/locate/colsurfa

Preparation of highly porous nitrogen-doped biochar derived from birch tree wastes with superior dye removal performance

Glaydson S. dos Reis [a,*], Davide Bergna [b], Alejandro Grimm [a], Eder C. Lima [c], Tao Hu [b], Mu. Naushad [d], Ulla Lassi [b]

[a] Department of Forest Biomaterials and Technology, Biomass Technology Centre, Swedish University of Agricultural Sciences, Umeå SE-901 83, Sweden
[b] Research Unit of Sustainable Chemistry, University of Oulu, P.O. Box 3000, FI-90014, Oulu, Finland
[c] Federal university of Rio Grand do Sul (UFRGS), Porto Alegre, RS, Brazil
[d] Department of Chemistry, College of Science, King Saud University, P.O. Box 2455, Riyadh, Saudi Arabia

HIGHLIGHTS

- Green strategy for developing advanced heteroatom-doped biomass-derived carbon materials.
- Nitrogen doping strategy boosted the number of functionalities on the biochar surface.
- Nitrogen doping boosted dye adsorption capacity due to the multiple mechanisms.

GRAPHICAL ABSTRACT

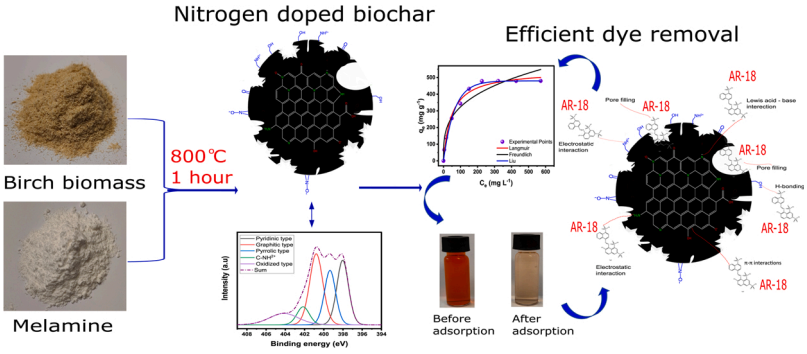

ARTICLE INFO

Keywords:
Birch tree wastes
Nitrogen doping
Nitrogen-doped biochar
Anionic dye removal
Lab-made dye effluent

ABSTRACT

Heteroatom doping is a highly effective strategy that can be used to modify carbonaceous adsorbents to improve their chemical reactivity and increase their adsorptive properties. Herein, a simple method is reported for the preparation of nitrogen-doped biochar using a natural and abundant biowaste from birch trees and melamine as a nitrogen dopant for the adsorption of Acid red 18 (AR-18) dye from water. The doped biochars were also characterized for their performance during the treatment of synthetic effluents. The physicochemical characterization results showed that the N-doping process provoked remarkable chances on the biochar morphology, pore structure, and surface functionalities. N-doped biochar showed abundant nitrogen functional groups with 5.4 % of N in its structure while non-doped carbon showed traces with 0.47 %. Moreover, the specific surface area of doped biochar was dominated by mesopores (86.4 %) while non-doped was dominated by micropores (67.8 %). Raman analysis showed that the incorporation of N created more defects in the biochar structure. The adsorption experiments showed that the N-doping boosted the biochar adsorptive performance. The maximum adsorption capacity of the doped biochar was 545.2 mg g^{-1}, while the non-doped exhibited 444.5 mg g^{-1}, i.e., an increase of 22.6 %. The kinetic and equilibrium studies showed that Avrami fractional order and Liu models were the most suitable for describing the experimental AR-18 dye adsorption data. The equilibrium parameters were

* Corresponding author.
E-mail address: glaydson.simoes.dos.reis@slu.se (G.S. dos Reis).

https://doi.org/10.1016/j.colsurfa.2023.131493
Received 14 February 2023; Received in revised form 3 April 2023; Accepted 19 April 2023
Available online 20 April 2023

found to obey a nonlinear relationship with the temperature. Since the biochars are highly porous, pore filling was the main adsorption mechanism, however; AR-18 dye removal suggests that interactions such as electrostatic, hydrogen bonds, Lewis acid-base, and π-π between the adsorbent and the dye are involved. The thermodynamic studies showed that the removal of the AR-18 dye from the solution is dependent on temperature, exothermic, and spontaneous. The N-doped biochar showed excellent removal performances of contaminants from synthetic effluents confirming their high efficiency for color removal. This research shows that N-doping is an efficient strategy to design effective, low-cost, and sustainable adsorbents to remediate dye contamination in wastewater.

1. Introduction

Contamination of water bodies by dyes from industrial wastes has become a serious environmental issue due to the toxicity and carcinogenicity features of these compounds [1,2]. Among several classes of dyes, azo (anionic) dyes, where the Acid red dye 18 fits in, are generally found in wastewater of dyeing industries [3]. They are widely used and highly soluble in water, which makes them dangerous to the environment and living organisms [3]. The presence of dyes in water negatively affects aquatic life by not allowing the proper penetration of sunlight and hindering photo-synthesis, thus causing eutrophication of lakes and rivers [3]. Research has shown that exposure to azo dyes can provoke skin issues and also lead to cancer and cell mutation in humans [3–5]. In addition, these types of dyes are worldwide-used and nearly 10–15 % of the dyes used in dying processes are discharged into sewage systems, or in the worst cases, into rivers. The toxicity and harm that these types of chemicals can cause to the environment are some of the reasons why their removal from industrial effluents is extremely important.

There are many methods for removing dyes from wastewater, including nano-filtration [6,7], reverse osmosis [7], electrocoagulation, and advanced oxidation methods [8,9]. However, such operations demand very high implementing/operating costs, lead to formation of by-products, and in many cases are inefficient. Among affordable, efficient, simple and well-known methods for removal of pollutants from water, adsorption with activated carbon/biochar is one of the best choices [10–13]. In general, well-developed pore structures and very high specific surface area (SSA) as well as surface functionalities are key factors for an efficient adsorption process [14].

Activated carbon/biochar adsorbents with different physicochemical and adsorptive properties can be easily produced from biomass wastes), resulting in the production of adsorbent materials with different physicochemical and adsorptive properties [10,14,15]. In addition, carbon materials are easily modified by doping heteroatoms (such as oxygen, nitrogen, sulphur, boron, and phosphorus) in their structures to improve their physicochemical and adsorptive properties. Besides, non-metal doping methods are sustainable, efficient, low-cost, and environment-friendly and suitable to replace toxic metals and their oxides [15–17].

Heteroatom doping is the most employed strategy to introduce functionalities on biomass-derived carbon surfaces [12–14], the heteroatom doping induces electron density changes that modify the polarity of the carbon surface, promoting the formation of binding sites for molecules or ions, and therefore, boosting their adsorption properties [16,18]. Nitrogen (N) is one of the most suitable heteroatoms for doping whereas N atoms are able to break the basic sp^2 -hybridized structure and create new active sites on carbon material structure [18,19]. Nitrogen doping often occurs within the graphitic planes and enhance the inner-plane defects by adjusting its internal configuration such as electron density of local carbon atoms, active sites, and surface functional groups that could boost its adsorptive properties through electrostatic interactions [18–20]. Also, N doping creates edge defects that can increase its porosity and therefore adsorptive properties [20].

Works dealing with nitrogen doping to boost the adsorption properties of activated biochars are available in the literature. Lian et al., [21] prepared N-doped microporous biochar from crop straws under the presence of NH_3 as a dopant agent. The doped biochar exhibited high microporosity (71.5 %) and 8.81 % of N in its structure. When tested as an adsorbent of dyes such as acid orange 7 and methyl blue, the doped biochar presented extremely better performance than non-doped (around 15 times higher). The authors stated that the N insertion into the biochar matrix changed its electron density distribution and created new surface functionalities, which resulted in better and stronger interactions between the doped surfaces and the dyes.

Herein, nitrogen-doped biochar was synthesized using birch tree wastes as a carbon precursor. The birch (*Betula spp*.) genus includes dozens of tree species densely distributed in North America, Asia and Europe, including northern Finland and Sweden [22]. Melamine was used as a nitrogen dopant, and the activation was done using single-step pyrolysis. Non-doped biochars were used for comparison. The effect of the doping on the biochar's final physicochemical properties was subjected to a deep investigation. The produced biochars were employed to remove Acid red 18 dye from aqueous solution and to treat synthetic effluents containing several dyes and pollutants usually found in wastewater. In practice, the idea is to develop a sustainable and green strategy to produce high-performance biomass adsorbent materials able to treat synthetic and real wastewater. The current knowledge has important gaps between the production of activated biochars from different biomass resources, employing different synthesis routes, and doping methods, and how these influence their physicochemical and adsorptive properties. Therefore, is expected that this research can help to reduce the gaps by directly correlating the carbon properties linking with its preparation and doping processes.

2. Materials and methods

2.1. Preparation of the activated biochars

Waste generated during harvest of birch (*Betula* spp.) trees grown in Umeå, Sweden was ground using a hammer mill equipped with a 1 mm sieve and used as such. The biochars were prepared according to the method described by Gonzalez-Hourcade et al. [20]. Briefly, the biomass samples were mixed with H_3PO_4 (50 wt. %) at a weight ratio of 1:4 (dried biomass:acid) plus 30 % of melamine (dry weight biomass:melamine), kneaded until a homogenous paste was formed, and dried in an oven at 80 °C overnight. For the non-doped biochar, the same procedure was used but without the addition of melamine. The impregnated samples were pyrolysed using a specially designed reactor at a temperature of 800 °C in a nitrogen atmosphere for 1 h. The temperature of the sample was increased at 10 °C/min. Finally, samples were ground using a hammer mill and sieved to a particle size range of < 200 μm. To wash away the remaining and by-products from the pyrolysed carbon materials, they were washed several times with boiling deionized water until the pH of the wash water was equal to the pH of the deionized water. Hereafter, these samples are named Non-doped biochar and N-doped biochar.

2.2. Characterization of the biochars

Specific surface area (SSA) and micro/meso pore structure were obtained using a sorptometer (Tristar 3000, Micromeritics Instrument

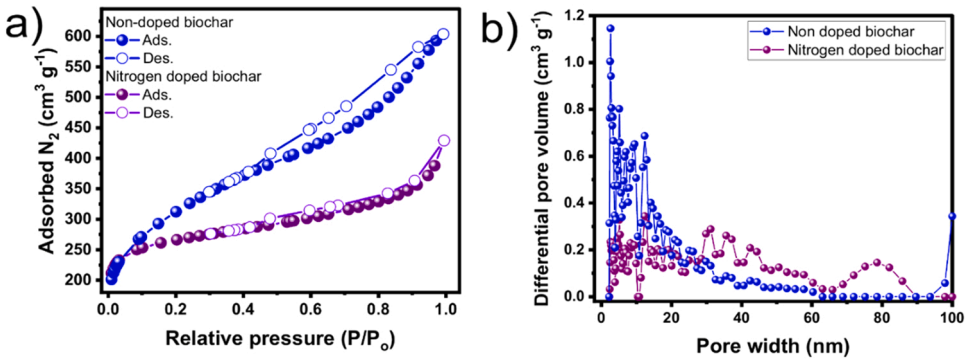

Fig. 1. a) N_2 adsorption-desorption isotherms and b) pore size distribution of the biochars.

Corp., Norcross, GA, USA). The SSA was calculated from Brunauer–Emmett–Teller (BET) method, and pore size distribution using the Barrett−Joyner−Halenda (BJH) model. X-ray photoelectron spectroscopy (XPS) was performed via a Kratos spectrometer following standard procedures. Raman spectra of the adsorbents were obtained using a Bruker Bravo spectrometer (Bruker, Ettlingen, Germany). The point of the zero charge (pH_{pzc}) value was obtained by plotting measured zeta potential value with pH measured via a Zetasizer Nano ZSE 3700 (Malvern Instrument Co., UK) at 298 K varying pH from 2 to 10. The elemental analysis of the birch biomass was performed using an elemental analyser (EA-IsoLink, Thermo Fisher Scientific). Shortly, 0.05 g oven-dried samples were used to determine total carbon (C), nitrogen (N), oxygen (O), and hydrogen (H) contents. The results showed contents of 48.56 %, 44.14 %, 5.88 % and 0.04 % of carbon, oxygen, hydrogen and nitrogen contents, respectively.

2.3. Adsorption studies

De-ionized water was used for the preparation of the AR-18 dye solutions. The batch mode was employed to evaluate the applicability of the non-doped and nitrogen doped biochars in removing AR-18 dye from aqueous solutions. The effect of the pH, initial dye concentration, and solution temperature on AR-18 dye adsorption were investigated. All adsosption experiments were performed using 30 mg of each biochar into 20 mL of AR-18 dye using 50.0 mL Falcon containers. For isotherms studies, AR-18 initial solution concentrations from 70 to 1000 mg L^{-1} were employed in the experiments. The effect of the pH was determined by varying the pH from 2 to 10. The kinetic AR-18 dye removal on biochars was studied varying contact time from 0 to 250 min with an AR-18 dye initial concentration of 500 mg L^{-1}. The effect of temperature and thermodynamic studies were performed at temperatures of 298, 308, and 318 K. All adsorption experiments were performed at a constant shaking speed of 200 rpm. After adsorption, the residual solutions of AR-18 were quantified using a UV-Visible spectrophotometer (Shimadzu 1800) at a maximum wavelength of 510 nm. The removal capacity and the percentage of AR-18 removal are obtained from Eqs. (S1 and S2), respectively (see Supplementary material).

2.4. Kinetics, equilibrium, and thermodynamics studies

Kinetic adsorption results were evaluated using pseudo-first-order (PFO), pseudo-second-order (PSO), and Avrami fractional-order models. Isotherms were explored using the nonlinear isotherm models of Freundlich, Langmuir, and Liu. The adsorption thermodynamics was attained by the van't Hoff approach, whose equilibrium constant was accessed from the best equilibrium constant obtained in the isotherms from 298 to 318 K. Details of these models are given in the Supplementary material.

Table 1
Surface area analysis of the biochars.

	SSA	A_{Micro}	A_{Meso}	Pore volume
	(m^2 g^{-1})			(cm^3 g^{-1})
Non-doped biochar	1086	736	266	0.8964
N-doped Biochar	1003	219	867	0.5791

2.5. Synthetic dye effluents

For the lab-made effluents, de-ionized water was used for the preparation the synthetic effluents containing several dyes and compounds as listed in Supplementary Table S1. Two different lab-made effluents with different compositions were prepared to evaluate the biochars' effectiveness for treating simulated real effluents.

3. Results and discussion

3.1. Biochars textural features

Among important features of an adsorbent, the specific surface area and pore structure play usually a huge weight on the adsorbent's adsorptive performance. N_2 adsorption isotherms and pore size distributions of the prepared biochars are displayed Fig. 1a, where is observed an obvious and significant difference in their pore structures and porosities.

Regarding N_2 adsorption isotherms, according to the IUPAC classification [23], the isotherm for the non-doped biochar seems to have a curve with a portion of type I (which is related to the microporous behavior), especially at low partial pressure that adsorbs high amounts of N_2. It also shows a portion of type IV (which is related to the presence of mesopores), which is highlighted by the presence of hysteresis. The N-doped biochar exhibits a curve closer to type IV, with a predominant presence of mesoporosity. However, both biochars show a combination of micro and mesopores in their structures.

The differences in textural properties suggested by N_2 isotherms are highlighted by the pore size distribution curves (Fig. 1b). Non-doped biochar shows larger quantities of small mesopores (from 2.6 to 10.0 nm), and micropores centred at 1.9 nm. The nitrogen-doped sample besides shows a large amount of small mesopores, and also portions of big mesopores from 25 to 50 nm as well as some macropores up to 85 nm. These values are in accordance with the N_2 isotherms, as previously discussed.

These differences in the pore size distribution could affect the S_{BET} of the biochars, which in turn, affect their adsorptive properties that are partially dependent on the pore structure of the adsorbents besides S_{BET}.

Table 1 shows the S_{BET}, A_{Micro}, and A_{Meso} of the biochars. The non-doped biochar has a higher S_{BET} compared to that of the N-doped biochar, although 7.4 % higher. A small difference, therefore, it can be

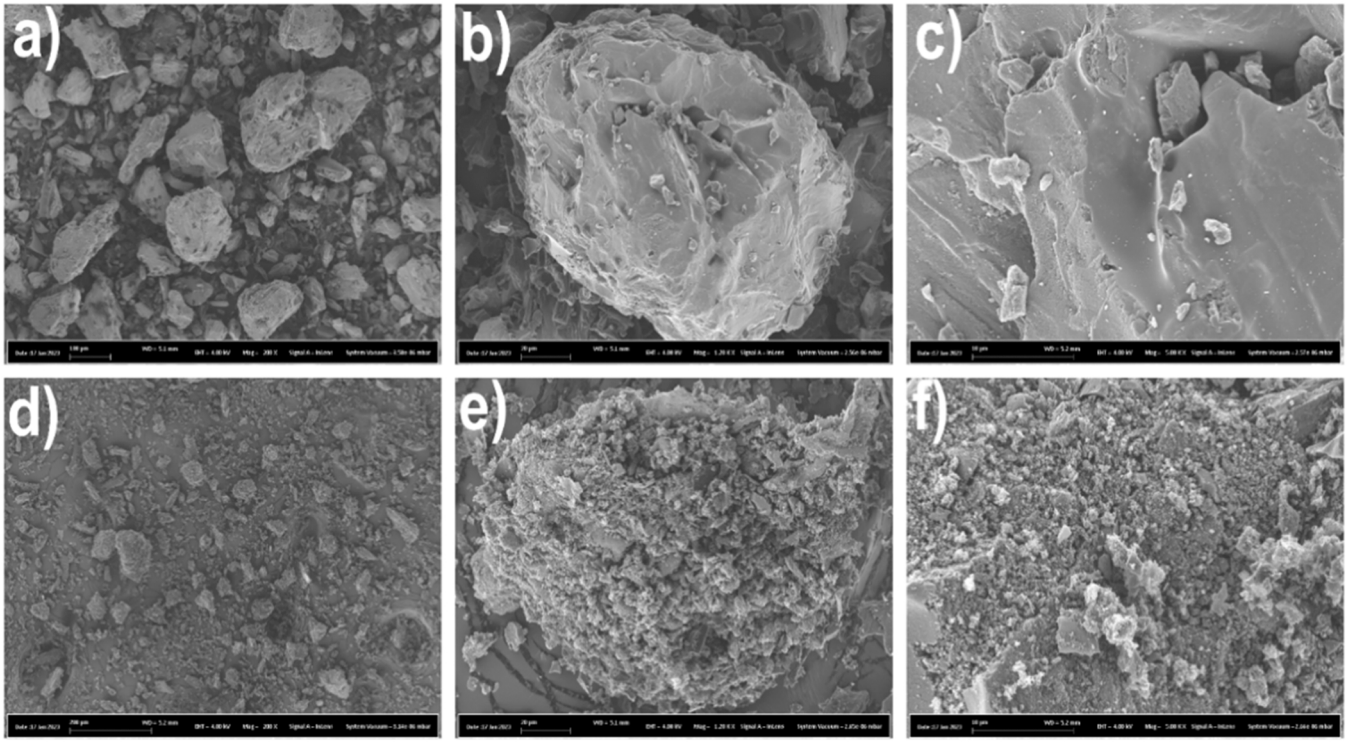

Fig. 2. SEM images at different magnifications (a, b and c) non-doped biochar and (d, e and f) for N-doped biochar.

stated that the doping process with nitrogen did not reduce the S_{BET} value to a large extent. However, it is in the pore structure that the N-doping showed to have more influence. The doped biochar exhibited a very high mesopore surface area equal to 867 m^2 g^{-1} (showing a structure composed of 86.4 % of mesopores) while non-doped biochar 67.8 % of micropores. Thus, it is obvious that nitrogen doping significantly influenced the biochar pore structure, which can also effectively influence its adsorptive performances. The reduction in the S_{BET} could be due to the collapse of some of the pore walls as the pore width increase leading to an increased mesoporosity [24]. It is reported that the introduction of nitrogen-containing substances during the modification of the biochar might cause the blockage of some micropores as well as its widening to become mesopores and therefore helping to reduce the S_{BET} that is largely contributed by the number of micropores [24,25].

Compared to S_{BET} values of doped biochar available in the literature, the surface area achieved in this work was higher than in many reports [20,21,25]. For instance, Li et al. [25] employed herb residue to produce nitrogen-doped biochar and the non-doped and N-doped biochar presented S_{BET} of 171.6 and 96.6 m^2 g^{-1}, respectively. Gonzalez-Hourcade et al. [20] prepared N-doped biochar from microalgae biomass and found that the N-doping increased the S_{BET} from 324 to 433 m^2 g^{-1}.

The surface morphology and textural features of the non-doped and N-doped biochar were analyzed using SEM-EDX analyses. The SEM images at different magnifications are shown in Fig. 2. The non-doped biochar showed particles with bigger sizes, smooth surfaces and much less roughness in comparison with N-doped biochar, which showed a rough structure. This indicates that nitrogen doping caused a strong influence on biochar morphology. Such difference could be attributed to the formation of a biochar's structure rich in defects upon the incorporation of nitrogen atoms into the graphitic carbon network, which could reflect better adsorptive performances. SEM images at higher magnification (125.000x) are shown in Supplementary Fig. S1. At this magnification, no obvious differences are observed, and both samples display very rough surface structure, suggesting these biochars are highly porous as indicated in both Fig. 1 and Table 1. Results of SEM analysis indicate that N-biochar with different textural properties has been successfully prepared.

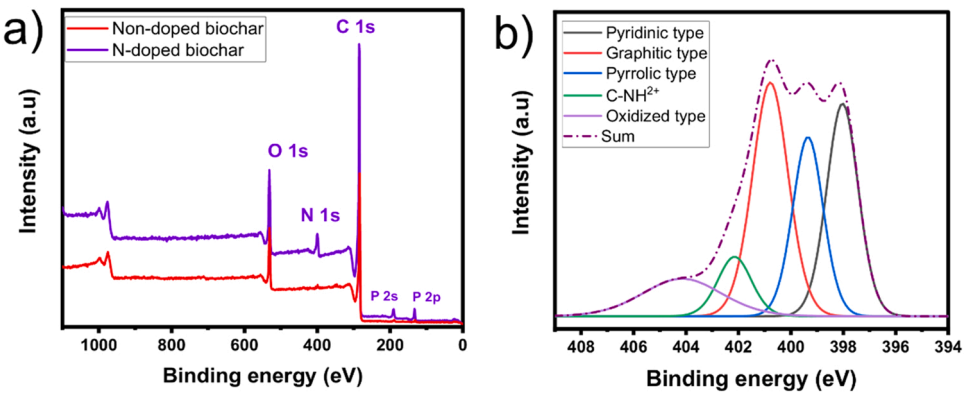

Fig. 3. a) XPS survey spectra for non-doped and N-doped biochars and b) deconvoluted N 1 s peaks.

Table 2
Biochars XPS elemental analysis (at. ratio %).

	XPS					N^1s state				
	C^1s	O^1s	N^1s	P^2p	N/C	N1	N2	N3	N4	N5
Non-doped biochar	86.51	8.95	0.47	0.90		0.12	0.10	0.15	-	0.10
N-doped-biochar	83.42	9.43	5.40	1.99		1.36	1.11	1.7	0.5	0.7

N1 = Pyridinic; N2 = Graphitic; N3 = Pyrrolic; N4 = C-NH^{2+};N5 = Oxidized

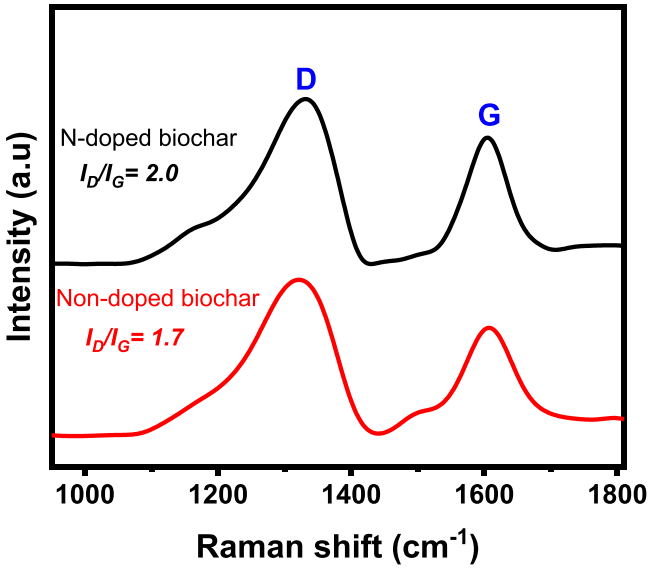

Fig. 4. Raman spectra of biochars.

3.2. Chemical composition of the biochars

The elemental compositions and chemical states of the biochars were determined by X–ray photoelectron spectroscopy (XPS). The XPS survey spectra of both biochars are shown in Fig. 3a. C 1 s, N 1 s, O 1 s, and P 2p, P 2 s were detected in doped biochar while N 1 s is not present in Non-doped biochar, which confirms the successful doping process.

Since the presence of N in non-doped biochar was very small (0.47 %, atomic ratio %, See Table 2), only the N 1 s spectra, of the doped biochar, is shown (See Fig. 3b). The spectra was deconvoluted into five peaks at 398.0 eV (pyridine-N), 399.3 eV (Graphitic-N), 400.8 eV (pyrrolic-N), 402.8 eV (C-NH^{2+}), and 404.2 eV (oxidized-N), respectively. As shown in Fig. 3 and Table 2, pyrrolic- and pyridine-like N are the main states in doped-biochar [20,26,27].

Table 2 shows that while only a trace of 0.47 % of N content is in non-doped, N-doped biochar possesses 5.4 % of N, which is higher than many N-doped biochars reported in the literature. Ji et al. [26], reported the preparation of doped biochar using marine algae as precursor; the doped biochars possessed nitrogen content ranging from 1.53 % and 3.47 %. Lin et al. [27] prepared N-doped carbon employing urea as N source with a biomass precursor: urea ratio of 1:0.5, and the resulting material exhibited a N amount of 3.4 % in its structure.

Table 2 also highlights the presence of phosphorous in both biochars that comes from the activation process that was made with H_3PO_4. The XPS analysis showed a large presence of O in both samples (being slightly higher in the doped sample). Nitrogen doping resulted in biochar rich in N and O, which may indicate a big amount of biochar surface functionalities, which often reflects better adsorptive properties.

So far, some characterization has proved that the N-doping provoked important changes in biochar structure; therefore, the effect of N-doping on biochar properties is further investigated by Raman analysis, which gives valuable information on the order/disorder and degrees of biochars graphitization [20,28,29].

Fig. 4 shows that both biochars showed two characteristic peaks at 1335 cm^{-1} (D-band) and 1610 cm^{-1} (G-band). The D-band is related to C atoms of defects or disordered structures, normally dominant in amorphous biochar made from biomass, while G-band represents carbon atoms with an sp^2 electronic configuration in graphite structures [20,28,29]. In addition, from Raman spectrum, the ratio between D and G peaks (I_D/I_G) is often employed to determine the degree of graphitization of the biochar.

The N-doped biochar showed higher I_D/I_G (2.0) compared to Non-doped biochar (1.7) (see Fig. 4), and therefore more defects and less graphitic structures. Generally, defects in the biochars/adsorbents could provide adsorption sites, which can be responsible for boosting their adsorptive properties. Therefore, nitrogen doping may have provided a biochar with better adsorptive performances.

3.3. Zeta potential (pH_{pzc}) and pH effect on AR-18 removal

The pH_{pzc} of the biochars was performed, indicating the point where the biochar's surface potential is equal to zero, which also indicates that values under pH_{pzc} the biochar surface charge is positive and above is negative. The effect of N-doping on surface zeta potentials of the biochars in relation to the pH of solution are compared in Fig. 5a. The pH_{pzc} of N-doped biochar was 5.2 which is more than the non-doped biochar

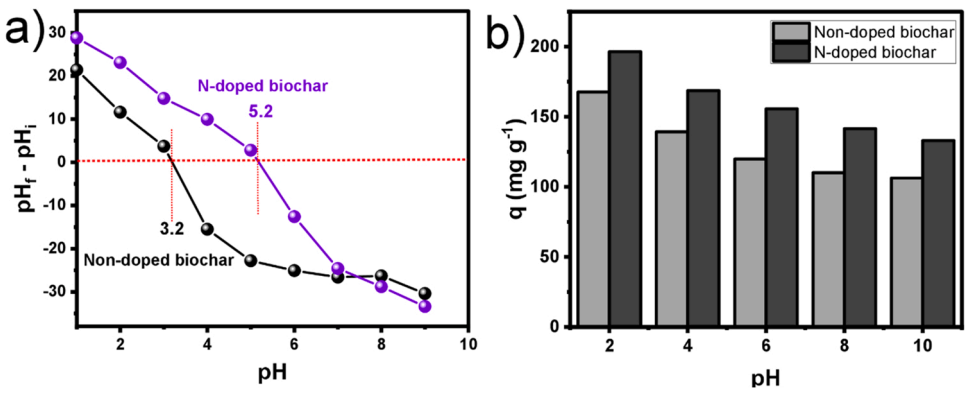

Fig. 5. a) Zeta potential and pH_{pzc} of the biochars, and b) effect of the pH on AR-18 dye removal.

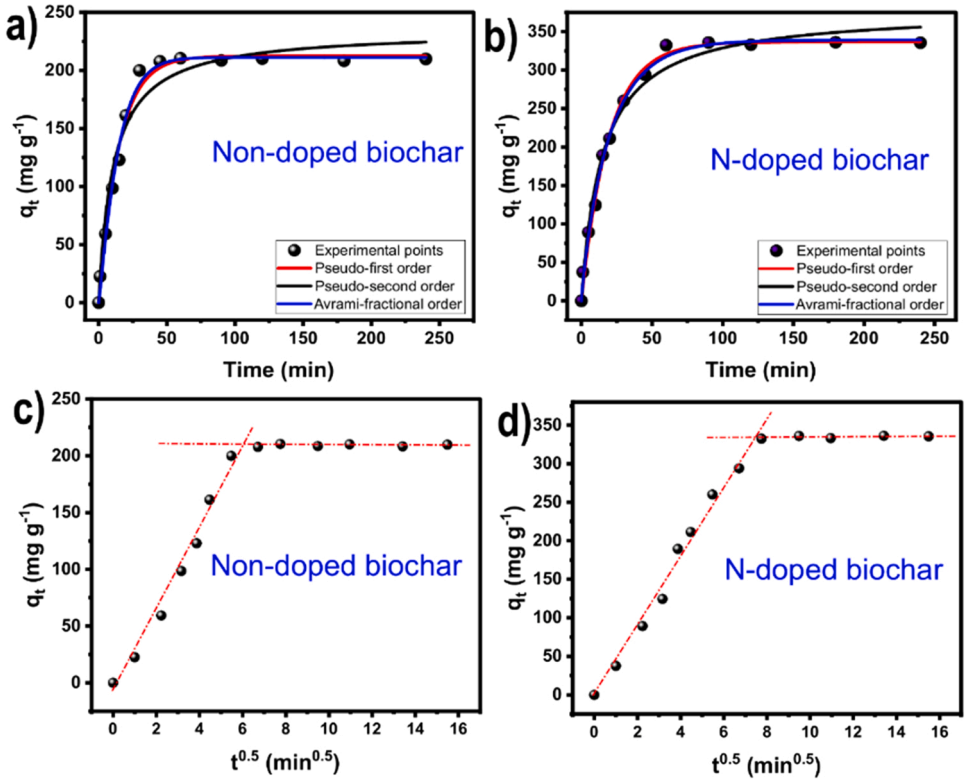

Fig. 6. Kinetic curves of AR-18 adsorption onto biochars. Experimental conditions: 400 mg L-1 of initial concentration, adsorbent dosage of 1.5 g L^{-1}, initial pH of 6.0 and 298 K:.

Table 3
Kinetic model results for AR-18 adsorption.

	Non-doped biochar	N-doped biochar
Pseudo-first order		
q_1 (mg g^{-1})	212.5	336.5
k_1 (min^{-1})	0.06749	0.05131
R^2_{adj}	0.9912	0.9936
SD (mg g^{-1})	7.362	9.810
Pseudo-second order		
q_2 (mg g^{-1})	234.4	378.2
k_2 (g mg^{-1} min^{-1})	0.0004968	0.0001761
R^2_{adj}	0.9654	0.9835
SD (mg g^{-1})	14.60	15.82
Avrami-fractional order		
q_n (mg g^{-1})	211.2	339.1
k_n [min^{-1} (g $mg^{-1})^{n-1}$]	0.06796	0.05029
n_{AV}	1.122	0.9170
R^2_{adj}	0.9922	0.9951
SD (mg g^{-1})	7.000	9.044

(3.2). The doping of biochar with nitrogen due to its low electronegativity (3.04) compared to oxygen (3.44), affects biochar surface chemistry and isoelectric point [30]. pH < pH_{pzc}, it would be favorable for the AR-18 anionic dye adsorption. This means that the N-doped biochar surface is positively charged at pH below 5.15, which favours the removal of anionic AR-18 [31–34].

The effect of the initial pH of AR-18 solution on the adsorption efficiency was investigated (see Fig. 5b). The initial pH was varied from 2 to 10 and it is observed that the pH did influence the AR-18 removal. AR-18 is an anionic dye with pKa <1 (See Supplementary Fig. S2), which comprises mainly sulfonic acid groups (R-SO_3Na) [33]. During the adsorption process, the positively charged groups of biochars were electrostatically attracted to AR-18 since it is an anionic dye. As the pH value of AR-18 solution increases, the AR-18 adsorption decreased due to the Coulombic repulsion between the negative surface charge from the nitrogen and PO_4^{3-} species of Biochars and the dominant SO_3^- species of AR-18 [33,34]. Besides, the reduced adsorption at higher pHs can also be attributed to the competition with OH− ions towards adsorption sites.

3.4. Kinetic Study

The kinetics of adsorption is one of the most crucial steps to evaluate the efficiency of an adsorbent during the adsorption process and, thus, it hugely determines the feasibility of the adsorption system and potential application of the adsorbents. The kinetics of AR-18 uptake on biochars were performed using pseudo-first order (PFO), pseudo-second order (PSO), and Avrami fractional order (AFO) models (equations shown in the Supplementary material). Fig. 6 shows the results from the measurements and Table 3 the parameters obtained from each model. It seems that the AR-18 molecules are rapidly adsorbed during the first 30 min for non-doped biochar and 45 min for the doped biochar. This difference could be due to the fact that N-doped biochar has more active sites that require more time to be filled up with AR-18 molecules, and then gradually reach equilibrium.

To examine the kinetic models fitness, R^2_{adj} and SD were evaluated. The model that gives the best fitting must exhibit the highest R^2_{adj} and lowest SD [35–37], meaning a smaller disparity among experimental and theoretical q values.

Form the results one can see that AFO was the most suitable, for both biochars. The AFO is a largely applied kinetic model to describe many different adsorption systems (different types of adsorbents – adsorbates) [35–37]. AFO suggests that the adsorption process is very complex with multiple pathways, with the possibility of changes in the adsorption mechanism, while it is taking place, by following multiple kinetic orders, which change during adsorbent–adsorbate contact [35–37]. The n_{AV} exponent suggests that the adsorption has multiple kinetic orders, and usually it has a fractional value [35,36].

Considering the complexity of the AFO, as above mentioned, the

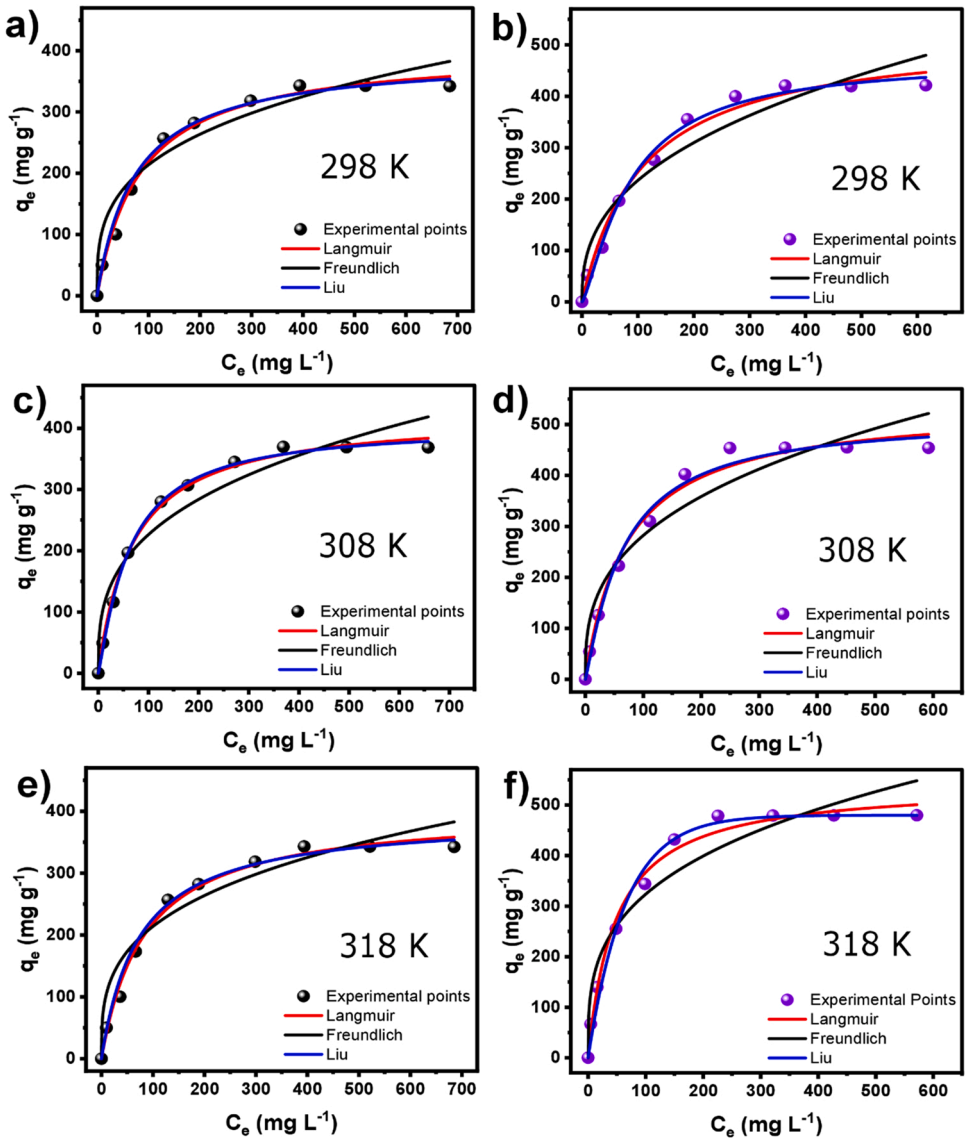

Fig. 7. Isotherms of adsorption for AR-18 on non-doped (a, c and e) and doped biochars (b, d and f) at different temperatures (298, 308 and 318 K). Experimental conditions: Adsorbent dosage of 1.5 g L^{-1}, initial pH of 6.0.

Table 4
Equilibrium model results for AR-18 adsorption.

Isotherm model	Non-doped biochar			Nitrogen-doped biochar		
	Temperature			Temperature		
	298 K	308 K	318 K	298 K	308 K	318 K
Langmuir						
q_e (mg g^{-1})	401.9	423.7	464.5	524.7	539.1	542.6
k_1 (min^{-1})	0.01191	0.01458	0.01532	0.009300	0.001920	0.02086
R^2_{adj}	0.9917	0.9960	0.9972	0.9869	0.9875	0.9889
SD (mg g^{-1})	11.92	8.888	8.159	18.87	20.10	19.79
Freundlich						
k_F ((mg g^{-1})(mg L^{-1})$^{-1/nF}$)	53.06	50.30	54.96	39.29	57.54	80.36
n_F (dimensionless)	3.304	3.062	3.031	2.566	2.896	3.306
R^2_{adj}	0.9399	0.9310	0.9334	0.9322	0.9249	0.9279
SD (mg g^{-1})	18.77	36.95	40.10	42.93	49.34	50.43
Liu						
Q_{max} (mg g^{-1})	391.2	403.4	444.5	471.1	514.2	545.2
Kg (L mg^{-1})	0.01370	0.01616	0.01685	0.01151	0.01528	0.02066
n_L (dimensionless)	1.000	1.150	1.130	1.298	1.137	0.9861
R^2_{adj}	0.9998	0.9971	0.9981	0.9899	0.9878	0.9895
SD (mg g^{-1})	6.421	7.524	6.653	16.55	18.22	17.96

Table 5
Comparison of the q_{max} for AR-18 dye using different adsorbents.

Adsorbents	q_{max} (mg g^1)	pH	Ref.
Granular ferric hydroxide	29.13	5.0	[34]
Chitosan- hydrogel composites	342.5	2.0	[38]
Chitosan films	194.6	7.0	[39]
Copper dithiocarbamate-modified starch	99.1		[40]
Magnetic Chitosan/Carbon Nanotube composites	771.1	3.0	[41]
Activated carbons peach $H_4P_2O_7$	34.24	3.0	[42]
Multiwall carbon nanotubes	166.6	3.0	[43]
Graphene oxide/zero-valent iron composites	26.6	2.0	[44]
Diethylenetriamine-modified starch	700.6	4.0	[45]
Non-doped biochar	444.5	6.0	This work
Nitrogen doped biochar	545.2	6.0	This work

intraparticle diffusion process was performed to evaluate the kinetic measurements by the rate-limiting step of the AR-18 removal process (see Fig. 6c and d). The adsorption of AR-18 was characterized by two-stage processes, i.e., fast initial adsorption to outer surfaces, followed by a slow diffusion into the inner pores of the carbons. In the first stage, the concentration of AR-18 was very high, which provided a large mass transfer force for diffusion. The curves show that doped carbon seems to have a longer first stage, maybe due to the presence of more adsorption sites and bigger pores, making a high adsorption rate for AR-18. For instance, N-doped carbon has a lot more mesopores than non-doped which is predominantly microporous, and bigger pores can accommodate more AR-18 molecules and therefore may need more time for the diffusion to take place. As the adsorption proceeded, the AR-18 concentration is reduced as well as the difference between the solid−liquid concentrations, which makes the adsorption rate diminish.

3.5. Equilibrium studies

Isotherm of adsorption is largely employed to understand the interaction between adsorbent- adsorbate system at optimum conditions. In addition, it helps to evaluate the effectiveness of an adsorbent because it gives its maximum adsorption capacity, and therefore, it is essential to design an efficient adsorption process. Thus, the isotherms of adsorption for AR-18 on non-doped and N-doped biochars were performed to evaluate the adsorption equilibrium process. To evaluate the effect of the temperature of the solution containing the dye on the adsorption, measurements were done at 298, 308 and 318 K. The Langmuir, Freundlich and Liu isotherm models were employed and discussed. The equations of each model are shown in the Supplementary material.

The isotherm curves and parameters are displayed in Fig. 7 and Table 4, respectively. Fig. 7 shows that for both carbons and all temperatures, the adsorbed amounts of AR-18 sharply enhanced as the initial concentration increased, due to the significant driving force from the concentration gradient to overcome the mass transfer resistance of AR-18 between the aqueous phase and solid phase.

The isotherm curves show that the N-doped biochar had better performance on AR-18 removal compared to non-doped biochar. These results are interesting because it shows that the adsorption process does not correlate only with the S_{BET} (non-doped had a S_{BET} 7.4 % higher) but also the nitrogen doping may have significantly influences in the AR-18 adsorption due to the incorporation of surface funcionalities already mentioned in XPS results.

The isotherm curves also show that the adsorption capacity increased as the temperature increased; however, the detailed explanation on the effect of temperature on AR-18 removal is further examined in the next section, thermodynamic studies.

The equilibrium models and their suitability was evaluated as made for the kinetic measurements. Thus, the Liu model resulted in the highest R^2_{adj} and lowest SD values, being then the best model to describe the adsorption equilibrium for AR-18 on both biochars at all studied temperatures. This suggests that the q_{max} from Liu model were very close to those found experimentally. Further comparing the other models, Freundlich shows a clear lack-off-fit and Langmuir parameters are very closer to Liu's parameters, which may suggest that AR-18 removal on biochars takes place mainly through monolayer adsorption on a homogeneous surface is assumed by the Langmuir model, with minimum interactions among AR-18 molecules and biochars.

Table 6
Thermodynamic parameters of AR-18 on biochar adsorbents.

T (K)	K (-)	ΔG^0 (kJ mol^{-1})	ΔH^0 (kJ mol^{-1})	ΔS^0 (kJ mol^{-1} K^{-1})
Non-doped biochar				
298	7706	-22.17	-8.202	102.1
308	9090	-23.34		
318	9478	-24.21		
Nitrogen doped biochar				
298	3430	-20.17	-23.10	145.0
308	4553	-21.57		
318	6157	-23.07		

3.6. Comparison of N-doped biochar q_{max} with the literature data

In Table 5 values of maximum adsorption capacity (q_{max}) of AR-18 dye for different types of adsorbents reported in the literature are compared to the results from this work. From the table, one can see that the q_{max} of the nitrogen-doped biochar is among the third-highest performances for AR-18 dye adsorption compared to the other adsorbents. The highest q_{max} value is 771.1 mg g^{-1}, which was achieved by an adsorbent based on Magnetic Chitosan/Carbon Nanotube composites, and although it presented a higher q_{max} value than N-doped biochar (545.2 mg g^{-1}), its production cost is much higher than N-doped biochar. Thus, considering that the cost of the adsorbent fabrication is an important parameter to observe, biomass-based doped biochars can be labelled as effective adsorbents to treat dye-polluted effluents.

3.7. Thermodynamic studies

To successfully evaluate the temperature effect on AR-18 adsorption, it is mandatory to obtain the thermodynamic process and its parameters. Thermodynamic studies of any adsorption process bring important insights regarding the nature of the adsorption process in terms of spontaneity, feasibility, randomness, exothermicity or endothermicity [46]. The Gibbs's free energy (ΔG°) is a fundamental parameter of the spontaneity of the adsorption system, and it can take place spontaneously whether ΔG° has a value >0. A positive standard entropy (ΔH°) value indicates that the adsorption phenomenon is endothermic, while a negative value means an exothermic adsorption process. The magnitude and sign of entropy (ΔS°) indicate the degree of randomness or disorder of the system.

Table 6 shows that ΔG° and ΔS° presented negative and positive values, respectively, meaning that the AR-18 removal on both biochars is spontaneous and favourable. Both biochars presented positive values for ΔS°, which suggests an increase in the randomness of the adsorption process at the solid/solution interface during the uptake of AR-18 dye molecules and suggests a high affinity between biochars and AR-18 dye. ΔH° for both biochars were negative, highlighting the exothermic nature of the removal of AR-18 on both biochars. The magnitude of enthalpy suggests that physical adsorption was the main mechanism involved in the process since its values are <40 kJ mol^{-1} [20,47].

3.8. Mechanism of adsorption for AR-18 dye on N-doped biochar

A mechanism of adsorption between AR-18 and N-doped biochar can be stated based on the biochars' physicochemical characteristics (porosity and chemical surface and functionalities) and adsorption

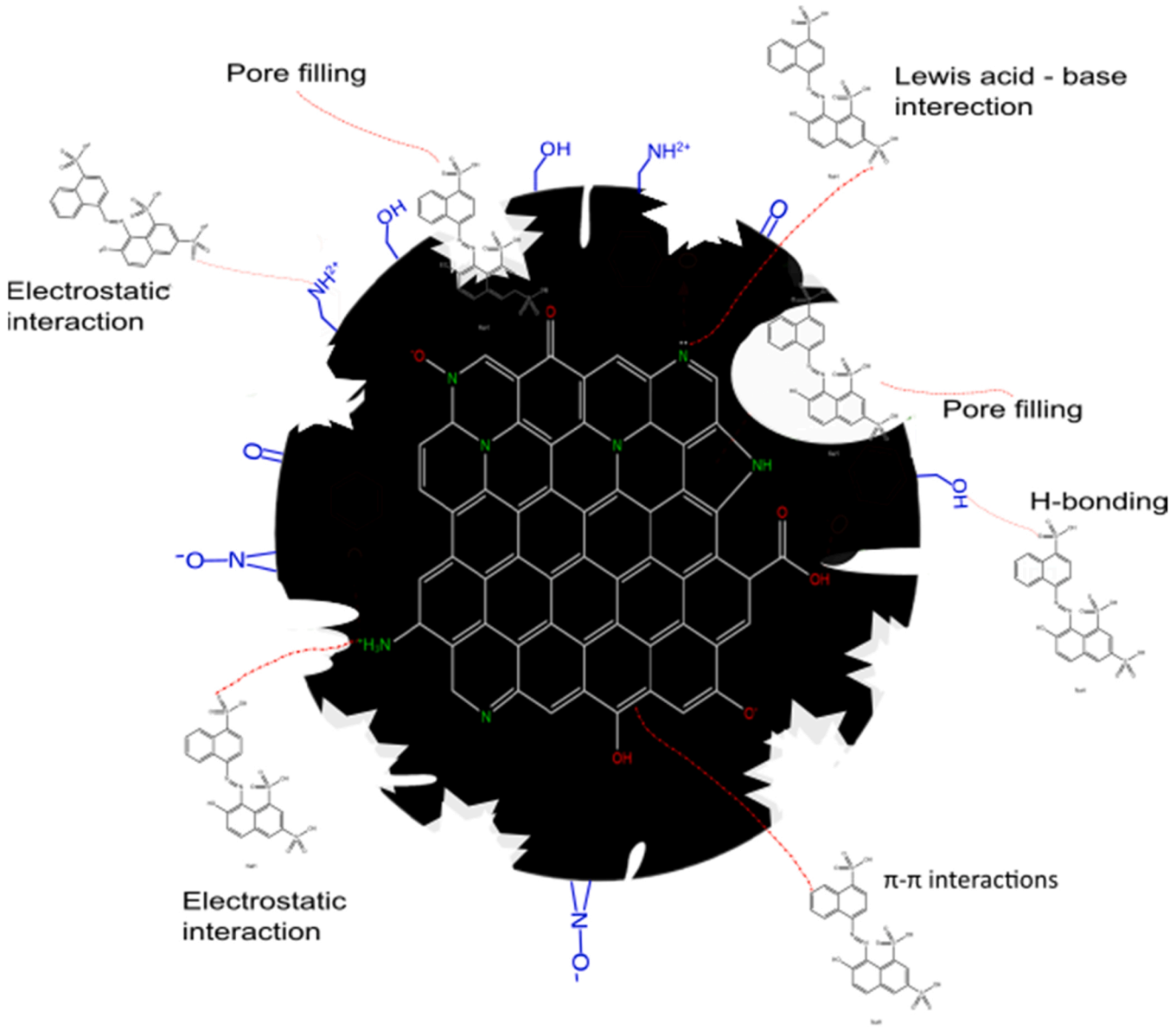

Fig. 8. Mechanism of adsorption involved in the AR-18 dye removal onto N-doped biochar.

results [18,47–49]. The high adsorption of AR-18 by the N-doped biochar was achieved due to physical effects (e.g., pore-filling mechanism) and chemical interactions (e.g., electrostatic attraction, H-bonding, $\pi - \pi$ interactions, Lewis acid-base interaction) [18], see Fig. 8. Since the biochars are very porous, physical adsorption through pore filling should be the principal mechanism involved in the process [10,36,37]

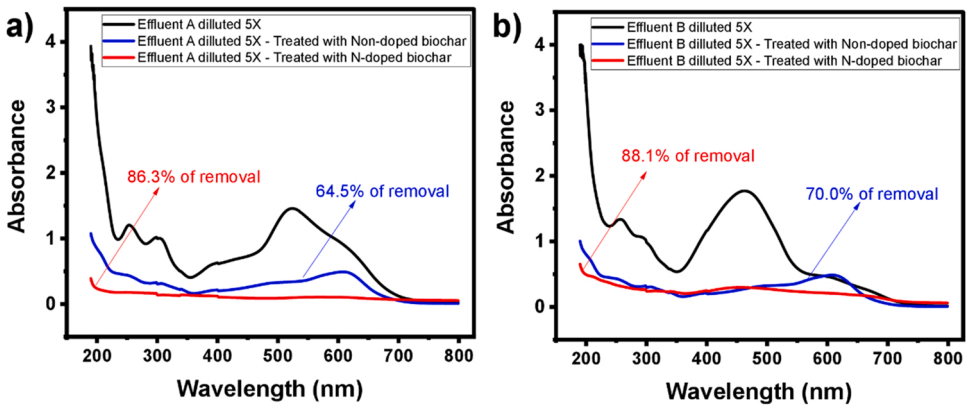

Fig. 9. Treatment of lab-made dyes effluent. **a**) Effluent A; **b**) Effluent B.

although other also takes place in removing AR-18 from the aqueous solution. Doping N on carbon matrix generates positive clouds due to electronegativity differences that boost the electrostatic attraction of anionic dyes such AR-18 [18]. For instance, Wang et al. [47] stated that N-functionalities withdrew the π-electrons from biochar's graphene layers, which created positive sites that acted as acceptors of π-electron that interact with aromatic rings of AR-18 (π-electron-enriched). Under acidic conditions and pHs lower than 3.2 and 5.2, for non-doped and doped biochars, respectively; the mechanism of AR-18 removal is based on unprotonated nitrogen groups (e.g., -NH_2) on doped biochar surface that are protonated to form $-NH_3^+$ positively charged groups electrostatically attracting the negatively charged $-SO_3^-$ group on AR-18 dye species [13].

At pH higher than 3.2 and 5.2 (for non-doped and doped biochar, respectively), other interaction such as hydrogen bonding contributes to the adsorption process that takes place among a hydrogen donor and acceptor present on the biochar surface (–NH_2, –OH, –COOH, O^-, etc.) [47,49]. Lewis acid–base interactions can also happen between N-doped biochar and AR-18, biochars have functionalities that might donate electrons (N- and O) and act as Lewis bases. Electrostatic interactions are also involved in the AR-18 dye removal that take place between moieties with opposite charges and this mechanism is dependent of solution pH.

3.9. Treatment of synthetic dye effluents

The adsorption experiments have proven that N-doped biochar was highly effective on removing AR-18 from aqueous solutions. This is a strong indicative that the biochars could also be effectively employed to treat colorful effluents. To obtain such outcome, lab-made effluents containing several dyes and other compounds, commonly found in real wastewaters, we made to test the effectiveness of the biochar in treating such effluents.

The UV–vis spectra of the lab-made effluents before and after the adsorption are displayed in Fig. 9. The efficiency of dyes and compounds removal were obtained calculating the spectra areas under the absorption bands from 190 to 800 nm [13,20,37,50,51]. The results showed that N-doped biochar removed 86.3 % and 88.1 % of the total compounds form lab-made effluents A and B, respectively; while non-doped biochar removed 64.5 % and 70 % for effluents A and B, respectively. Such differences match with the previous adsorption results that pointed out that N-doped biochar exhibited better adsorptive performance. Taking into account that the lab-made effluents can be considered similar to the real dying effluents, it can be stated that the biochars prepared in this work could be effectively employed in real wastewater treatment.

4. Conclusions

The low-cost nitrogen-doped biochar was fabricated through a green and simple strategy and efficiently employed for the removal of AR-18 dye from aqueous solutions and lab-made effluents. The concept of using nitrogen was to increase the overall surface activity of biochar by creating new functionalities that acted as active binding sites for dye removal. N-doped biochar exhibited much higher N content (5.4 %) compared to the non-doped biochar (0.47 %), which results in abundant nitrogen surface functionalities. Moreover, the nitrogen doping strategy generated highly mesoporous biochar while non-doped was predominantly microporous. The adsorption experiments showed that the N-doping boosted the biochar adsorptive performance. The maximum adsorption capacity of the N-doped biochar 545.2 mg g^{-1} while non-doped exhibited 444.5 mg g^{-1}, a performance 22.6 % better. The kinetic and equilibrium studies showed that Avrami fractional order and Liu models better described the AR-18 dye kinetic and equilibrium results. AR-18 dye removal suggests that the main adsorption mechanism is pore filling, although that many interactions are involved. The thermodynamic studies indicated that the adsorption process on biochars is dependent on the temperature and is endothermic and spontaneous. With regards to the applicability of the biochars for treating lab-made effluents, N-doped biochar showed excellent treatment performances confirming their high efficiency for dye adsorption. This research shows that N-doping is an efficient strategy to design effective, low-cost and sustainable materials to remediate wastewaters polluted with dyes.

CRediT authorship contribution statement

Glaydson S. dos Reis: Conceptualization, Software, Data curation, Investigation, Methodology, Writing – original draft. **Davide Bergna**: Software, Analyses, Writing – review & editing. **Alejandro Grimm:** Formal analysis, Writing – review & editing. **Eder C. Lima**: Writing – review & editing. **Tao Hu**: Formal analysis, review & editing. **Mu. Naushad**: Writing – review & editing. **Ulla Lassi**: Writing – review & editing, Funding acquisition.

Declaration of Competing Interest

The authors declare that they have no known competing financial interests or personal relationships that could have appeared to influence the work reported in this paper.

Data Availability

No data was used for the research described in the article.

Acknowledgments

Dr. dos Reis thanks Bio4Energy - a Strategic Research Environment appointed by the Swedish government and the Swedish University of Agricultural Sciences, for the funding support. Dr. Alejandro Grimm acknowledges financial support from the Swedish Research Council FORMAS (2021–00877). The authors are grateful to the Researchers Supporting Project number (RSP2023R8), King Saud University, Riyadh, Saudi Arabia, for the financial support. The FT-IR and Raman measurements were performed at the Vibrational Spectroscopy Core Facility (ViSp), Chemical Biological Centre (KBC), Umeå University.

Appendix A. Supporting information

Supplementary data associated with this article can be found in the online version at doi:10.1016/j.colsurfa.2023.131493.

References

[1] R. Al-Tohamy, S.S. Ali, F. Li, K.M. Okasha, Y.A.-G. Mahmoud, T. Elsamahy, H. Jiao, Y. Fu, J. Sun, A critical review on the treatment of dye-containing wastewater: ecotoxicological and health concerns of textile dyes and possible remediation approaches for environmental safety, Ecotoxicol. Environ. Saf. 231 (2022), 113160.
[2] B. Adomas, L. Sikorski, A. Bęs, K. Warminski, Exposure of Lemna minor L. to gentian violet or Congo red is associated with changes in the biosynthesis pathway of biogenic amines, Chemosphere 254 (2020), 126752.
[3] S.H. Hashemi, M. Kaykhaii, Chapter 15 - Azo dyes: sources, occurrence, toxicity, sampling, analysis, and their removal methods, in: T. Dalu, N.T. Tavengwa (Eds.), Emerging Freshwater Pollutants, Elsevier, 2022, pp. 267–287, https://doi.org/10.1016/B978-0-12-822850-0.00013-2.
[4] S. Parmar, S. Daki, S. Bhattacharya, A. Shrivastav, Microorganism: an ecofriendly tool for waste management and environmental safety. Development in Wastewater Treatment Research and Processes, Elsevier,, 2022, pp. 175–193.
[5] K.T. Chung, Azo dyes and human health: a review, J. Environ. Sci. Health C. Environ. Carcinog. Ecotoxicol. Rev. 34 (2016) 233–261.
[6] P.S. David, A. Karunanithi, N.N. Fathima, Improved filtration for dye removal using keratin–polyamide blend nanofibrous membranes, Environ. Sci. Pollut. Res. 27 (2020) 45629–45638.
[7] S.K. Nataraj 1, K.M. Hosamani, T.M. Aminabhavi, Nanofiltration and reverse osmosis thin film composite membrane module for the removal of dye and salts from the simulated mixtures, Desalination 249 (2009) 12–17.
[8] M. Thanavel, P.O. Bankole, R. Selvam, S. Prabhu, S.K. Sadasivam, Synergistic efect of biological and advanced oxidation process treatment in the biodegradation of Remazol yellow RR dye, Sci. Rep. 10 (2020) 20234.

[9] S. Golmohammadi, M. Ahmadpour, A. Mohammadi, A. Alinejad, N. Mirzaei, M. Ghaderpoori, A. Ghaderpoori, Removal of blue cat 41 dye from aqueous solutions with ZnO nanoparticles in combination with US and US-H2 O2 advanced oxidation processes, Environ. Health Eng. Manag. J. 3 (2) (2016) 107–113.
[10] G.S. dos Reis, S.H. Larsson, M. Thyrel, T.N. Pham, E.C. Lima, H.P. de Oliveira, G. L. Dotto, Preparation and application of efficient biobased carbon adsorbents prepared from spruce bark residues for efficient removal of reactive dyes and colors from synthetic effluents, Coatings 11 (7) (2021) 772.
[11] R.A. Teixeira, E.C. Lima, A.D. Benetti, P.S. Thue, M.R. Cunha, N.F.G.M. Cimirro, F. Sher, M.H. Dehghani, G.S. dos Reis, G.L. Dotto, Preparation of hybrids of wood sawdust with 3-aminopropyl-triethoxysilane. Application as an adsorbent to remove Reactive Blue 4 dye from wastewater effluents, J. Taiwan Inst. Chem. Eng. 125 (2021) 141–152.
[12] Y.L. de, O. Salomon, J. Georgin, G.S. dos Reis, E.C. Lima, M.L.S. Oliveira, D.S. P. Franco, M.S. Netto, D. Allasia, G.L. Dotto, Utilization of Pacara Earpod tree (Enterolobium contortisilquum) and Ironwood (Caesalpinia leiostachya) seeds as low-cost biosorbents for removal of basic fuchsine, Environ. Sci. Pollut. Res 27 (2020) 33307–33320.
[13] E.H.M. Cavalcante, I.C.M. Candido, H.P. de Oliveira, K.B. Silveira, T.V.S. Álvares, E.C. Lima, M. Thyrel, S.H. Larsson, G.S. dos Reis, 3-Aminopropyl-triethoxysilane-functionalized Tannin-Rich grape biomass for the adsorption of methyl orange dye: synthesis, characterization, and the adsorption mechanism, ACS Omega 7 (2022) 18997–19009.
[14] G.S. dos Reis, S.H. Larsson, M. Thyrel, M. Mathieu, P.N. Tung, Application of design of experiments (DoE) for optimised production of micro-and mesoporous Norway spruce bark activated carbons, Biomass. Conv. Bioref. (2021), https://doi.org/10.1007/s13399-021-01917-9.
[15] A. Sanchez-Sanchez, F. Suarez-Garcia, A. Martinez-Alonso, J.M.D. Tascon, Synthesis, characterization and dye removal capacities of N-doped mesoporous carbons, J. Colloid Interface Sci. 450 (2015) 91–100.
[16] G.S. Dos Reis, H.P. de Oliveira, S.H. Larsson, M. Thyrel, E.C. Lima, A short review on the electrochemical performance of hierarchical and nitrogen-doped activated biocarbon-based electrodes for supercapacitors, Nanomaterials 11 (2021).
[17] L. Liang, X. Niu, X. Han, C. Chang, J. Chen, Salt sealing induced in situ N-doped porous carbon derived from wheat bran for the removal of doxycycline from aqueous solution, Environ. Sci. Pollut. Res. 29 (2022) 49346–49360.
[18] N. Kasera, P. Kolar, S.G. Hall, Nitrogen-doped biochars as adsorbents for mitigation of heavy metals and organics from water: a review, Biochar 4 (2022) 17.
[19] S. Ye, G. Zeng, X. Tan, H. Wu, J. Liang, B. Song, N. Tang, P. Zhang, Y. Yang, Q. Chen, X. Li, Nitrogen-doped biochar fiber with graphitization from Boehmeria nivea for promoted peroxymonosulfate activation and non-radical degradation pathways with enhancing electron transfer, Appl. Catal. B Environ. 269 (2020), 118850.
[20] M. Gonzalez-Hourcade, G.S. dos Reis, A. Grimm, V.M. Dinh, E.C. Lima, S. H. Larsson, F.G. Gentili, Microalgae biomass as a sustainable precursor to produce nitrogen-doped biochar for efficient removal of emerging pollutants from aqueous media, J. Clean. Prod. 348 (2022), 131280.
[21] F. Lian, G. Cui, Z. Liu, L. Duo, G. Zhang, B. Xing, One-step synthesis of a novel N-doped microporous biochar derived from crop straws with high dye adsorption capacity, J. Environ. Manag. 176 (2016) 61–68.
[22] J. Hynynen, P. Niemistö, A. Viherä-Aarnio, A. Brunner, S. Hein, P. Velling, Silviculture of birch (*Betula pendula* Roth and *Betula pubescens* Ehrh.) in northern Europe, Forestry 83 (2010) 103–119.
[23] M. Thommes, K. Kaneko, A.V. Neimark, J.P. Olivier, F. Rodriguez-Reinoso, J. Rouquerol, Physisorption of gases, with special reference to the evaluation of surface area and pore size distribution (IUPAC technical report), Pure Appl. Chem. 87 (2015) 1051–1069.
[24] S. Liu, X. Feng, Z. Liu, W. Zhao, Y. Li, J. Zhang, Nitrogen doping in porous biochar from cotton stalk with H_3PO_4 activation for reduction of NOx with NH_3-SCR at low temperatures: Characteristics and catalytic activity analysis, Fuel 332 (2023), 126256.
[25] X. Li, J. Wang, L. Xia, R. Cheng, J. Chen, J. Shang, Peroxymonosulfate activation by nitrogen-doped herb residue biochar for the degradation of tetracycline, J. Environ. Manag. 328 (2023), 117028.
[26] R. Ji, Y. Wu, Y. Bian, Y. Song, Q. Sun, X. Jiang, L. Zhang, J. Han, H. Cheng, Nitrogen-doped porous biochar derived from marine algae for efficient solid-phase microextraction of chlorobenzenes from aqueous solution, J. Hazard Mater. 407 (2021), 124785.
[27] S. Lin, X. Yang, L. Liu, A. Li, G. Qiu, Electrosorption of cadmium and arsenic from wastewaters using nitrogen-doped biochar: mechanism and application, J. Environ. Manag 301 (2022), 113921.
[28] M. Pawlyta, J. Rouzaud, S. Duber, Raman microspectroscopy characterisation of carbon blacks: spectral analysis and structural information, Carbon 84 (2015) 479–490.
[29] V. Piergrossi, C. Fasolato, F. Capitani, G. Monteleone, G. Postorino, P. Gislon, Application of Raman spectroscopy in chemical investigation of impregnated activated carbon spent in hydrogen sulfde removal process, Int. J. Environ. Sci. Technol. 16 (2019) 227–1238.
[30] P. Alimohammadi, M.S. Nejad, M.R. Miroliaei, H. Sheibani, Oriented growth of copper & nickel-impregnated δ -MnO2 nanofilaments anchored onto sulfur-doped biochar template as hybrid adsorbents for removing phenolic compounds by adsorption-oxidation process, Chem. Eng. Process. - Process. Intensif. 176 (2022), 108971.
[31] J.S. Piccin, M.L.G. Vieira, J.O. Goncalves, G.L. Dotto, L.A.A. Pinto, L.A. A, Adsorption of FD&C Red No. 40 by chitosan: isotherms analysis, J. Food Eng. 95 (2009) 16–20.
[32] A. Roy, S. Chakraborty, S.P. Kundu, B. Adhikari, S.B. Majumder, Adsorption of Anionic-Azo dye from aqueous solution by lignocellulose-biomass jute fiber: equilibrium, kinetics, and thermodynamics study, Ind. Eng. Chem. Res. 51 (2012) 12095–12106.
[33] S. Subramaniam, K.Y. Foo, E.N. Md Yusof, Ali H. Jawad, L.D. Wilson, S. Sabar, Hydrothermal synthesis of phosphorylated chitosan and its adsorption performance towards Acid Red 88 dye, Int. J. Biol. Macromol. 193 (2021) 1716–1726.
[34] F. Hamidi, M.H. Dehghani, M. Kasraee, M. Salari, L. Shiri, A.H. Mahvi, Acid red 18 removal from aqueous solution by nanocrystalline granular ferric hydroxide (GFH); optimization by response surface methodology & genetic-algorithm, Sci. Rep. 12 (2022) 4761.
[35] É.C. Lima, D. Pinto, M. Schadeck Netto, G.S. Dos Reis, L.F.O. Silva, G.L. Dotto, Biosorption of Neodymium (Nd) from aqueous solutions using Spirulina platensis sp. Strains, Polymers 14 (2022) 4585.
[36] N.F.G.M. Cimirro, E.C. Lima, M.R. Cunha, P.S. Thue, A. Grimm, G.S. dos Reis, N. Rabiee, M.R. Saeb, F. Keivanimehr, S. Habibzadeh, Removal of diphenols using pine biochar. Kinetics, equilibrium, thermodynamics, and mechanism of uptake, J. Mol. Liq. 364 (2022), 119979.
[37] M. Guy, M. Mathieu, I.P. Anastopoulos, M.G. Martínez, F. Rousseau, G.L. Dotto, H. P. de Oliveira, E.C. Lima, M. Thyrel, S.H. Larsson, G.S. dos Reis, Process parameters optimization, characterization, and application of KOH-activated Norway spruce bark graphitic biochars for efficient azo dye adsorption, Molecules 27 (2022) 456.
[38] S.P. Zhao, F. Zhou, L.Y. Li, M.J. Cao, D.Y. Zuo, H.T. Liu, Removal of anionic dyes from aqueous solutions by adsorption of chitosan-based semi-IPN hydrogel composites, Compos. Part B: Eng. 43 (2012) 1570–1578.
[39] G.L. Dotto, J.M. Moura, T.R.S. Cadaval, L.A.A. Pinto, Application of chitosan films for the removal of food dyes from aqueous solutions by adsorption, Chem. Eng. J. 214 (2013) 8–16.
[40] R.M. Cheng, S.J. Ou, B. Xiang, Y.J. Li, Q.Q. Liao, Equilibrium and molecular mechanism of anionic dyes adsorption onto copper (II) complex of dithiocarbamate-modified starch, Langmuir 26 (2009) 752–758.
[41] S. Wang, Y.-Y. Zhai, Q. Gao, W.-J. Luo, H. Xia, C.-G. Zhou, Highly efficient removal of Acid Red 18 from aqueous solution by magnetically retrievable chitosan/carbon nanotube: batch study, isotherms, kinetics, and thermodynamics, J. Chem. Eng. Data 59 (2014) 39–51.
[42] R.G. Saratale, Preparation of activated carbons from peach stone by H4P2O7 activation and its application for the removal of Acid Red 18 and dye containing wastewater, J. Environ. Sci. Health Part A 51 (2016) 164–177.
[43] M. Shirmardi, A. Mesdaghinia, A.H. Mahvi, S. Nasseri, R. Nabizadeh, Kinetics and equilibrium studies on adsorption of acid red 18 (Azo-Dye) using multiwall carbon nanotubes (MWCNTs) from aqueous solution, E-J. Chem. 9 (2012) 2371–2383.
[44] H. Xu, H, et al., Reduced graphene oxide/attapulgite-supported nanoscale zero-valent iron removal of acid red 18 from aqueous solution, Water Air Soil Pollut. 229 (2018) 1–16.
[45] Z.H. Wang, B. Xiang, R.M. Cheng, Y.J. Li, Behaviors and mechanism of acid dyes sorption onto diethylenetriamine-modified native and enzymatic hydrolysis starch, J. Hazard. Mater. 183 (2010) 224–232.
[46] E.C. Lima, A. Hosseini-Bandegharaei, J.C. Moreno-Piraján, T. Anastopoulos, A critical review of the estimation of the thermodynamic parameters on adsorption equilibria. Wrong use of equilibrium constant in the Van't Hoof equation for calculation of thermodynamic parameters of adsorption, J. Mol. Liq. 273 (2019) 425–434.
[47] L. Wang, W. Yana, C. Hea, H. Wen, Z. Cai, Z. Wang, Z. Chen, W. Liu, Microwave-assisted preparation of nitrogen-doped biochars by ammonium acetate activation for adsorption of acid red 18, Appl. Surf. Sci. 433 (2018) 222–231.
[48] X.F. Li, K.Y. Lian, L. Liu, Y. Wu, Q. Qiu, J. Jiang, M. Deng, Y. Luo, Unraveling the formation mechanism of graphitic nitrogen-doping in thermally treated graphene with ammonia, Sci. Rep. 6 (2016) 1–10.
[49] Y. Li, B. Xing, X. Wang, Nitrogen-doped hierarchical porous biochar derived from corn stalks for phenol-enhanced adsorption, Energy Fuels 33 (2019) 12459–12468.
[50] F.M. Kasperiski, E.C. Lima, G.S. dos Reis, J.B. da Costa, G.L. Dotto, S.L.P. Dias, M. R. Cunha, F.A. Pavan, C.S. Correa, Preparation of CTAB-functionalized Aqai stalk and its efficient application as adsorbent for the removal of direct blue 15 and direct red 23 dyes from aqueous media, Chem. Eng. Commun. 205 (2018) 1520–1536.
[51] P.M. Carijo, G.S. dos Reis, E.C. Lima, G.L. Dotto, Functionalization of corn stover with 3-aminopropyl-triethoxysilane to uptake Reactive Red 141 from aqueous solutions, Environ. Sci. Pollut. Res. 26 (26) (2019) 32198–32208.